Structure–function relations in supported Ni–W sulfide hydrogenation catalysts

L. Vradman and M.V. Landau

Blechner Center for Industrial Catalysis and Process Development, Chemical Engineering Department, Ben-Gurion University of the Negev, Beer-Sheva 84105, Israel

Received 15 May 2001; accepted 31 July 2001

Ni–W catalysts were prepared by impregnation of commercial γ-alumina and silica supports. The sulfidation, performed directly after drying at 100 °C, yielded fully sulfided Ni–W species on both supports (SEM-EDAX, XPS, XRD). At optimal metals loading (~50 wt% NiO + WO_3, Ni/W = 2), the sulfided catalysts had similar texture (N_2 adsorption) and displayed similar activity in dibenzothiophene hydrodesulfurization (DBT HDS), while the activity of the Ni–W/SiO_2 catalyst in toluene hydrogenation (HYD) was six times higher than that of Ni–W/Al_2O_3. This is due to the more than two times higher WS_2 slabs stacking number in Ni–W/SiO_2 compared with Ni–W/Al_2O_3 (XRD, HR-TEM), yielding stronger adsorption of toluene (TPD).

KEY WORDS: Ni–W–S catalyst; DBT hydrodesulfurization; toluene hydrogenation; morphology; TEM; TPD; γ-alumina and silica supports

1. Introduction

Mo- and W-based hydrotreating catalysts, promoted by Co or Ni, are widely used in the oil industry for the removal of organo-sulfur and organo-nitrogen contaminants and aromatics hydrogenation. The structure–function relations in the Co–Mo sulfide catalysts have been extensively studied [1,2]. There is a general agreement that the active Co–Mo–S phase is MoS_2 slab with Co atoms decorating the edge plane. Recently, Lauristen *et al.* [3] obtained the first atomic-scale images of this Co–Mo–S structure. A few studies of the Ni–W system pointed out that the structure of the Ni–W–S active phase is similar to that of Co–Mo–S [1].

It is well established that Mo(W)S_2 are layered compounds consisting of stacks of S–Mo(W)–S layers held together by van der Waals interactions [1]. It is also generally agreed that the most active HDS catalysts contain highly dispersed active phase [1,2]. However, the effect of the stacking degree of Mo(W)S_2 on the catalyst activity in HYD and HDS reactions is still unclear. Indeed, only the length of Mo(W)S_2 slabs should affect the amount (dispersion) of the active sites, while the stacking degree should not, since the active sites are located on the edge planes of the slabs. In addition, apparently there is no reason for the layers to contain different types of the active sites since they are not chemically bonded, but held together by van der Waals interactions. However, according to the "rim-edge" model, proposed by Daage and Chianelli [4] for unsupported MoS_2, the basal plane of MoS_2 slab is inactive and there are two different types of active sites at the edge plane: rims (the top and bottom layer of the slab) and edges (layers in between). They found that the HDS reaction was catalyzed by both the rim and edge sites, while HYD is catalyzed predominantly by rim sites. Opposite to that, Hensen *et al.* [5] found that HYD rate increases with an increasing stacking degree of supported MoS_2. The present study aimed to clarify the effect of stacking degree on the performance of the Ni promoted WS_2 catalyst. The reason of using Ni–WS_2 catalyst is twofold. First, W-based catalysts are more active in HYD compared with Mo-based catalysts. High intrinsic HYD activity should assist in pronouncing the effect of stacking degree on HYD activity of the catalyst. Second, no information about the effect of stacking degree on the performance of the Ni promoted WS_2 catalyst is available in the literature. The understanding of this effect should give ideas for improving the HYD performance of the catalyst.

The bulk Ni–W mixed sulfide system is known as the most active non-noble sulfur-tolerant HYD catalyst [6]. The maximum HYD activity is obtained with an atomic ratio Ni/W = 2 [6,7]. Furthermore, in order to reach highest activity the sulfidation of the mixed oxide system should be performed directly after drying and without calcination [8–11]. Supported Ni–W catalysts could perform better than unsupported. The optimal Ni/W ratio for alumina supported Ni–W catalysts varied in the wide range from 0.6 to 1.5 [9,12–15] and is much higher than the well-known optimal ratio of 0.3–0.5 for Co–Mo and Ni–Mo hydrotreating catalysts [1,2]. Interaction between the support and active phase precursors should affect the state of the active phase depending on the support nature. In the present study, the preparation conditions yielding an optimized bulk Ni–W phase were employed for the first time for synthesis of supported catalysts on γ-alumina and silica. Because the metal–support interactions with γ-alumina and silica are substantially different we expected to prepare catalysts with different structure (stacking degree) of sulfide phase for clarifying the structure–function relations. The HDS and HYD activity of supported

1011-372X/01/1100-0047$19.50/0

Ni–W catalysts was measured using DBT and toluene as model compounds. SEM-EDAX, XPS, XRD and HR-TEM were used to study the state, dispersion and stacking degree of the Ni–W–S supported phase. The adsorption strength of toluene was measured by TPD.

2. Experimental

2.1. Catalyst preparation

Two commercial supports: γ-alumina (Norton SA 6175, cylinders $d = 1.3$ mm, BET surface area 270 m^2/g, pore volume 0.65 cm^3/g) and silica (PQ CS-1030E, cylinders $d = 1.7$ mm, BET surface area 300 m^2/g, pore volume 1.0 cm^3/g) were used in this study. Catalysts were prepared by wet impregnation of both supports with aqueous solution containing Ni-nitrate hexahydrate (Fluka), ammonium (meta) tungstate hydrate (Fluka) and citric acid (Aldrich), followed by drying at 60 °C for 16 h and at 100 °C for 24 h. Citric acid (at a molar ratio citric acid : Ni of 0.5) was used as a complexing agent that is effective in the depolymerization of polytungstate anions and that promotes the effective coordination of nickel around tungsten species [16]. This should improve the Ni–W homogenization at the molecular level favoring the formation of an active Ni–W–S phase during sulfidation.

2.2. Catalyst characterization

The chemical composition of the catalysts (wt%, average of five measurements at different points of the solid) was measured by the SEM-EDAX method (JEM-35 microscope, Jeol, Co., link system ANB-1000, Si–Li detector). The distribution of Ni–W on the support was measured by SEM-EDAX scanning along the cross section of the pellets. Less than 20% deviation from the average value was obtained in EDAX profiles of Ni and W for both Ni–W/Al_2O_3 and Ni–W/SiO_2.

Surface areas, pore volumes and pore size distributions were obtained from N_2 adsorption–desorption isotherms using the conventional BET and BJH methods. The samples were outgassed under vacuum at 250 °C. Isotherms were measured at liquid nitrogen temperature with a NOVA-1000 (Quantachrome, Version 5.01) instrument.

A PHI 549 SAM/AES/XPS ultrahigh vacuum (10^{-9} Torr) apparatus with double cylindrical mirror analyzer (CMA) and Mg Kα (1253.6 eV) X-ray source was used for recording the XPS spectra. Samples were powdered and mounted on an indium foil. After recording the general survey spectra, high-resolution scans were taken at a pass energy of 25 eV for the major peaks: C 1s, Ni 2p, W 4f, Al 2p, Si 2p, S 2p and O 1s. Quantitative analysis was based on published empirical atomic sensitivity factors [17].

Wide-angle XRD patterns were collected on a Philips diffractometer PW 1050/70 (Cu Kα radiation) with graphite monochromator. The data were recorded with 0.02° step size, 2 s at every step. The WS_2 crystal domain size h along the c-axis was determined using the Scherrer equation $h = K\lambda/[(B^2 - \beta^2)^{0.5}\cos(2\theta/2)]$, where the shape factor $K = 0.76$, $\lambda = 0.154$ nm, β is the instrumental broadening correction and B is (002) reflection broadening at $2\theta = 14.32°$. The apparent average number of layers (stacking number) was calculated using $n = h/(c/2)$, where $c = 12.362$ Å is the parameter of the hexagonal cell (JCPDS, powder diffraction file number 8-237 [18]). The Ni_3S_2 crystal domain size was determined using the Scherrer equation using the (113) reflection broadening at $2\theta = 49.902°$.

The high-resolution TEM (HR-TEM) micrographs were recorded using a JEM 2010 microscope operated at 200 kV and equipped with linked EDS. The samples for HR-TEM were prepared by depositing a drop of an ultrasonicated ethanol suspension of solid catalyst on a carbon-coated Cu grid. The grid was dried at 80 °C and mounted on a specimen holder. Samples were examined as grain mounts. The statistical analysis was proceeded using ten different places (100 × 100 nm) of the sample. The average particle length L was calculated according to the first moment of the distribution: $L = \sum_{i=1}^{m} m_i l_i / \sum_{i=1}^{m} m_i$, where l represents the length of the slab along the basal plane as determined directly from the HR-TEM picture, m is the number of particles measured in a size range. The average stacking number was calculated in the same manner using stacking number n instead of l in the first moment of the distribution equation. The same analysis for MoS_2- and WS_2-based catalysts was performed in previous studies [19,20].

The temperature-programmed desorption (TPD) measurements were carried out with an AMI-100 catalyst characterization system (Zetion-Altamira). Catalysts were impregnated in excess of toluene at room temperature and kept for 24 h. Then the samples were dried at 80 °C for 2 h. TPD spectra were recorded in a He flow of 25 cm^3/min over 0.2 g of the catalyst. Temperature of the sample was increased from 40 to 400 °C (5.5°C/min) and kept at 400 °C for 2 h. TPD spectra of catalysts that do not contain toluene were also collected since catalysts may contain adsorbed water and hydrogen disulfide [21]. These TPD spectra of "clean" catalysts were then subtracted from the TPD spectra of preadsorbed toluene.

2.3. Testing of catalyst performance

The catalyst performance measurements were carried out in a high-pressure, fixed-bed reactor mini-pilot unit, controlled automatically by a PC that was described in detail elsewhere [22]. 5 cm^3 of catalyst mixed with 10 cm^3 of 0.2 mm silicon carbide particles (Norton, Co.) were packed in a 12 mm ID stainless-steel tubular reactor between two 10 cm layers of 0.2 mm diameter silicon carbide particles.

All catalysts were sulfided before performance measurements for 24 h with a 1.5% dimethyldisulfide–toluene mixture at LHSV = 2.5 h^{-1}, 320 °C, a hydrogen pressure of 5.4 MPa and a H_2/toluene ratio 500 Nl/l.

The DBT HDS was carried out with 1 wt% DBT dissolved in a 50 wt% *n*-decane–50 wt% *n*-octadecane mixture at 320 °C, hydrogen pressure 3.1 MPa, H_2/liquid ratio of 500 Nl/l and LHSV in the range 40–120 h^{-1}. At selected conditions the DBT HDS rate fits pseudo-zero-order HDS kinetics [23]. The DBT HDS rate constants were calculated according to the equation $K_{HDS} = x_{DBT}\text{LHSV}$, where $K = k/C_0$ (C_0 – inlet DBT concentration, k – pseudo-zero-order HDS rate constant).

The toluene HYD experiments were conducted with a 1.5% dimethyldisulfide–toluene mixture at 355 °C, hydrogen pressure 5.4 MPa and H_2/toluene ratio of 1500 Nl/l. The toluene to methylcyclohexane conversion (x_{tol}) was measured using the same GC equipment as for DBT HDS products. At selected conditions, the HYD rate of toluene fits pseudo-first-order kinetics, as reported previously [24]. The toluene HYD rate constants were calculated according to the equation $K_{HYD} = \text{LHSV}\ln(1 - x_{tol})^{-1}$.

3. Results and discussion

3.1. Effect of support type, Ni/W ratio and Ni–W loading on catalyst HDS and HYD activity

The effect of Ni/W ratio on catalysts activity was investigated on series of silica and alumina supported catalysts containing 34 wt% WO_3 and Ni/W ratios from 0.3 to 2. It was found that maximal catalysts activity is obtained at Ni/W ratio of 2. The HYD activity of the optimized Ni–W/SiO_2 catalyst was 2.4 times higher and HDS activity was by 30% higher than that of the catalyst with Ni/W ratio of 0.3. This result is in agreement with high optimal Ni/W ratio for unsupported [6,7] as well as for supported Ni–W catalysts reported in [13–15].

Figure 1 demonstrates the effect of metals loading on toluene HYD and DBT HDS activities of Ni–W catalysts prepared by impregnation of silica (denoted Ni–W/SiO_2) and γ-alumina (denoted Ni–W/Al_2O_3). In all samples the Ni/W ratio was kept constant and equal to 2. The 100% loading sample represents an unsupported Ni–W catalyst, prepared by evaporation of the impregnation solution and drying the solid in the same way as the supported catalysts. Both silica and γ-alumina-supported catalysts displayed similar HDS activity at any loading level (figure 1(a)). The HDS activity increases with Ni–W loading up to a maximum around 50% loading. At loadings of >20%, the supported catalysts activity is higher than that of the unsupported catalyst.

In contrast to HDS activity, the HYD activity of the γ-alumina-supported Ni–W catalyst increased only slightly with increasing Ni–W loading (figure 1(b)). On the other hand, the HYD activity of the silica-supported catalyst sharply increased with Ni–W loading up to an optimal level of about 50% loading (figure 1(b)). At this loading, the HYD activity of the silica-supported catalyst was six times higher than that of γ-alumina-supported catalyst and bulk Ni–W.

Attempts to explain the difference in HYD activity of Ni–W/SiO_2 and Ni–W/Al_2O_3 catalysts by simple reasons like,

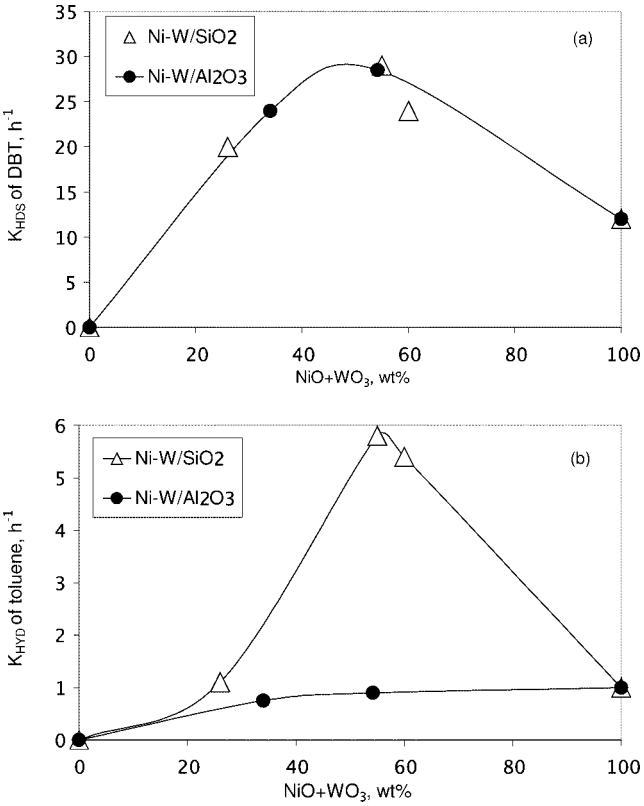

Figure 1. Effect of metals loading on HDS (a) and HYD (b) activity of Ni–W/SiO_2 and Ni–W/Al_2O_3 catalysts.

for example, poor Ni–W phase dispersion, incomplete sulfidation or pore blocking in case of Ni–W/Al_2O_3, fails to explain the DBT HDS results. In order to resolve this apparent contradiction, a set of characterization techniques was employed to investigate the structure and chemisorption ability of silica- and γ-alumina-supported Ni–W catalytic systems.

3.2. Characterization of Ni–W/Al_2O_3 and Ni–W/SiO_2 catalysts

Table 1 compares the results obtained by different characterization techniques with Ni–W/Al_2O_3 and Ni–W/SiO_2 catalysts. The samples had the same Ni–W content, as determined by SEM-EDAX before sulfidation. After sulfidation, the sulfur-to-metals atomic ratio was similar for both catalysts. Furthermore, this ratio was close (even slightly higher) to the theoretical stoichiometric ratio corresponding to Ni_3S_2 and WS_2 mixture, taking into account Ni/W = 2. This implies the same sulfidation degree of the Ni–W phase, which is close to its full sulfidation. The slight excess of sulfur at the surface of Ni–W/Al_2O_3 catalyst was also detected elsewhere [9] and it could be a result of the presence of WS_3 intermediates or formation of a stable mixed phase containing more sulfur than characteristic for Ni_3S_2.

N_2 adsorption–desorption measurements showed that both Ni–W/Al_2O_3 and Ni–W/SiO_2 catalysts after sulfidation have similar surface areas, pore volumes and pore diameters (table 1). The pore volume of silica decreased from 1.0 to 0.37 cm^3/g, whereas the pore volume of alumina only de-

Table 1
Catalysts characterization

Characterization technique	Catalyst	
	Ni–W/Al_2O_3	Ni–W/SiO_2
Chemical composition, *SEM-EDAX*, oxide form		
NiO (wt%)	20.9	21.1
WO_3 (wt%)	33.3	33.9
S/(Ni + W) (after sulfidation)	1.15	1.16
N_2 adsorption–desorption, sulfided catalysts		
Surface area (m^2/g)	158	180
Pore volume (cm^3/g)	0.29	0.37
Average pore diameter (nm)	7.3	8.2
XPS, sulfided catalysts		
Ni/Al(Si)	0.26	0.06
W/Al(Si)	0.14	0.08
Binding energy Ni $2p_{3/2}$ (eV)	854.2	854.3
Binding energy W $4f_{7/2}$ (eV)	32.6	32.6
XRD, sulfided catalysts		
Phase composition	Ni_3S_2, WS_2, γ-Al_2O_3	Ni_3S_2, WS_2
Average Ni_3S_2 crystal domains (nm)	4.1	10
Average WS_2 crystal domains size along *c*-axis (nm)	1.7	3.9
Average number of WS_2 layers (stacking number)	2.8	6.3
HR-TEM, sulfided catalysts		
Average surface density of WS_2 slabs, particles/1000 nm^2	14	3
Average particle length (nm)	7.3	7.7
Average stacking number	2.4	5.1

creased from 0.65 to 0.29 cm^3/g. This is a result of partial pore plugging of the silica support caused by larger particles of Ni–W sulfided phases on the silica than on the alumina (as will be shown below).

X-ray photoelectron spectroscopy was employed to investigate the sulfidation degree of the Ni–W surface species. The W spectrum (not shown) of silica-supported catalyst showed a single W 4f doublet at 32.6 eV, characteristic for WS_2 [25]. No other peaks were detected. This means that all W surface species are fully sulfided to WS_2. This is in agreement with data reported in [26] which demonstrated that in a silica-supported uncalcined Ni–W system W sulfide formation is complete at temperatures between 300 and 350 °C (sulfidation in the present work was conducted at 320 °C). The Ni 2p spectrum (not shown) exhibited a doublet with a binding energy of 854.3 eV that is close to that of the Ni 2p core level state in Ni_3S_2 [25]. Also in this case no other peaks where detected. Therefore, it can be concluded that the Ni species are fully sulfided as well. The same results were measured even at the lower sulfidation temperature of 150 °C [26]. W 4f and Ni 2p core levels of the Ni–W/Al_2O_3 catalyst showed behavior similar to corresponding core levels in Ni–W/SiO_2 (table 1). Calcination of the oxide Ni–W/Al_2O_3 system increases its stability against sulfidation [9–11]. Furthermore, it was found that in a catalyst dried at 100 °C both WS_2 and Ni–W–S formation occurs upon sulfidation at 300 °C [11]. In the present study catalysts were not calcined, only dried at 100 °C, so that sulfidation at 320 °C was sufficient to form fully sulfided Ni–W species. Thus, the XPS results demonstrated the full sulfidation of Ni–W components deposited on both silica and γ-alumina supports in agreement with the sulfur-to-metals ratio determined by SEM-EDAX.

Based on the metal-to-Al(Si) atomic ratios measured by XPS (table 1), the dispersion of Ni–W sulfided species at the catalyst surface was much higher in Ni–W/Al_2O_3 compared with Ni–W/SiO_2. The W/Al ratio is almost 100% higher and the Ni/Al ratio is more than four times higher compared with the corresponding W/Si and Ni/Si ratios. The different Ni(W)/Al and Ni(W)/Si ratios measured by XPS could be also caused by non-uniform distribution of Ni and W in the bulk of the support pellets (different for silica and alumina supports). We detected homogeneous distribution of Ni and W in both silica and alumina pellets (SEM-EDAX). In addition, recording the XPS spectra of the powdered samples should avoid any effect of non-homogeneous metals distribution in the bulk of the support pellets on the XPS data (even if there were any), taking into account that the XPS method collects averaged information from the sample area of about 2 mm^2. In order to avoid the effects of different molecular weight of the supports, kinetic energies of the characteristic electrons, the escape depth, support density and surface area on the interpretation of the XPS results, the measured metal-to-support ratios should be compared with corresponding theoretical ratios for monolayer dispersion, calculated according to the Kerkhof–Moulijn model [27]. Such calculations yielded the Ni/Al ratio of 0.29 and the Ni/W ratio of 0.15 for the Ni–W/Al_2O_3 catalyst, and ratios of 0.39 and 0.21, respectively, for the Ni–W/SiO_2 catalyst. The metal-to-Al ratios, predicted by the model, are similar to those

measured by XPS (table 1). Opposite to that, metal-to-Si ratios measured by XPS are 2.6–6 times lower than those predicted by the model. Therefore, the XPS results imply high dispersion of Ni–W sulfide phase on the alumina surface and poor dispersion on the silica surface. The lower Ni–W dispersion on silica than on γ-alumina is probably a result of the stronger interaction of Ni–W precursors with γ-alumina than with silica. This is in full agreement with the generally observed lower active phase dispersion on silica than on γ-alumina for Mo- and W-based supported systems prepared by impregnation [1,28,29]. Furthermore, the higher W/Al ratio compared with W/Si implies a lower stacking degree of the WS_2 slabs on γ-alumina compared with silica, as was reported for Co–Mo–S phase [30].

XRD measurements showed only two Ni–W containing phases: Ni_3S_2 and WS_2 (table 1). This confirms full sulfidation of Ni–W species supported by both silica and γ-alumina in agreement with the SEM-EDAX and XPS measurements. The presence of a separate Ni sulfide phase is a result of the high Ni/W ratio used in the present study. The appearance of a separate Ni sulfide phase was detected also in [8], where high Ni/W ratios of 1–2 were used. The dispersion of the sulfide phases is much higher in case of γ-alumina support than of the silica as could be seen from the average Ni_3S_2 and WS_2 crystal domain sizes calculated from XRD data (table 1). Both the Ni_3S_2 and WS_2 average crystal domain size were 2.3–2.4 times higher for the Ni–W/SiO_2 catalyst than for the Ni–W/Al_2O_3 catalyst. This is in agreement with lower Ni–W dispersion on silica compared with γ-alumina, detected by XPS. XRD also allows calculation of the apparent number of WS_2 layers – the stacking number. It is equal to 6.3 for Ni–W/SiO_2 and 2.8 for Ni–W/Al_2O_3 (table 1) due to higher WS_2 average crystal domains size along the c-axis for Ni–W/SiO_2 compared with Ni–W/Al_2O_3.

Figure 2 shows the HR-TEM micrographs of Ni–W/SiO_2 (a) and Ni–W/Al_2O_3 ((b) and (c)) catalysts at equal loading level shown in table 1. Typical WS_2 layer-like structures could be recognized in both samples. However, comparison of figure 2 (a) and (b), which are micrographs of Ni–W/SiO_2 and Ni–W/Al_2O_3, respectively, at the same magnification, clearly demonstrated the significant difference in surface concentration and structure of surface sulfided species supported on silica or γ-alumina. First of all, it could be seen that the surface concentration of sulfided species in the Ni–W/SiO_2 catalyst (a) is much lower compared to Ni–W/Al_2O_3 (b). The high surface concentration of sulfided species in the Ni–W/Al_2O_3 catalyst (amount of crystals per surface units) could be seen also in figure 2(c) with lower magnification. There is no proper way to quantify the WS_2 dispersion using HR-TEM mainly because of two reasons:

– not all sulfided species can be detected by HR-TEM – only those that are orientated with their layers more or less parallel to the direction of the electron beam;
– the WS_2 layer-like particles will not be recognized when the sample located at the proper points of the grid is too thick.

However, assuming random geometric orientation of surface species relatively to the direction of the electron beam allows us to claim a significant difference in WS_2 dispersion between Ni–W/Al_2O_3 and Ni–W/SiO_2 catalysts, based on visual comparison of figure 2 (a) and (b). It should be mentioned that figure 2 shows typical HR-TEM images. Generally, the same pictures were obtained on more than ten different places (100 $\times$ 100 nm) of the sample. The statistical approach, proposed in [10], includes calculation of surface density of WS_2-like slabs as number of particles per 1000 nm^2. The average density, calculated over ten different points (100 $\times$ 100 nm) of the sample, is equal to 3 and 14 for the Ni–W/SiO_2 and Ni–W/Al_2O_3 catalysts, respectively (table 1). Comparable results for an alumina-supported Ni–W system, which was sulfided at 340 °C directly after drying at 120 °C, were obtained in [10]. Since the surface area of both Ni–W/SiO_2 and Ni–W/Al_2O_3 catalysts is nearly similar (table 1), the higher WS_2 slab density on the γ-alumina support relative to silica points for a higher dispersion level of sulfided species in the γ-alumina-supported catalyst compared with silica. The lower dispersion of sulfided species in the silica-supported catalyst compared with Ni–W/Al_2O_3 as follows from the HR-TEM results is in full agreement with the XPS and XRD data reported above. In addition, HR-TEM allows particle length and stacking number to be measured. The results of particle length and stacking number distribution for the silica- and γ-alumina-supported Ni–W catalysts are presented in figure 3. The particle length distribution is similar for both catalysts (figure 3(a)) giving an average length of 7.7 nm for Ni–W/SiO_2 and 7.3 nm for Ni–W/Al_2O_3 (table 1). In spite of that, the stacking number distribution is very different and shifted to higher values for the Ni–W/SiO_2 catalyst with respect to Ni–W/Al_2O_3 (figure 3(b)). The average stacking number for Ni–W/SiO_2 is equal to 5.1, while that for Ni–W/Al_2O_3 is equal to 2.4. This is in good agreement with the XRD results, which gave stacking numbers of 6.3 and 2.8 for the Ni–W/SiO_2 and Ni–W/Al_2O_3 catalysts, respectively (table 1). Similarly, Hensen *et al.* [5] reported a much higher stacking degree in silica-supported Mo sulfide than in an alumina-supported catalyst. However, they measured a higher average slab length for silica-supported MoS_2 than for alumina-supported MoS_2. This could be the result of the different behavior of the Ni-promoted WS_2 system used in the present study compared with unpromoted MoS_2 or different preparation and sulfidation conditions.

The same HDS and different HYD activity of Ni–W/Al_2O_3 and Ni–W/SiO_2 catalysts, reported in the previous section, should be attributed to the main difference between these two catalysts: different WS_2 slab thickness. The total amount of active sites should be similar on both supports since the WS_2 slabs are of the same length and the active sites are located on the edge planes. The similar amount of active sites along with similar HDS activity of both catalysts implies that the HDS reaction occurs at the same rate at all WS_2 layers. However, the much higher HYD activity of the Ni–W/SiO_2 catalyst suggests that the aromatics HYD

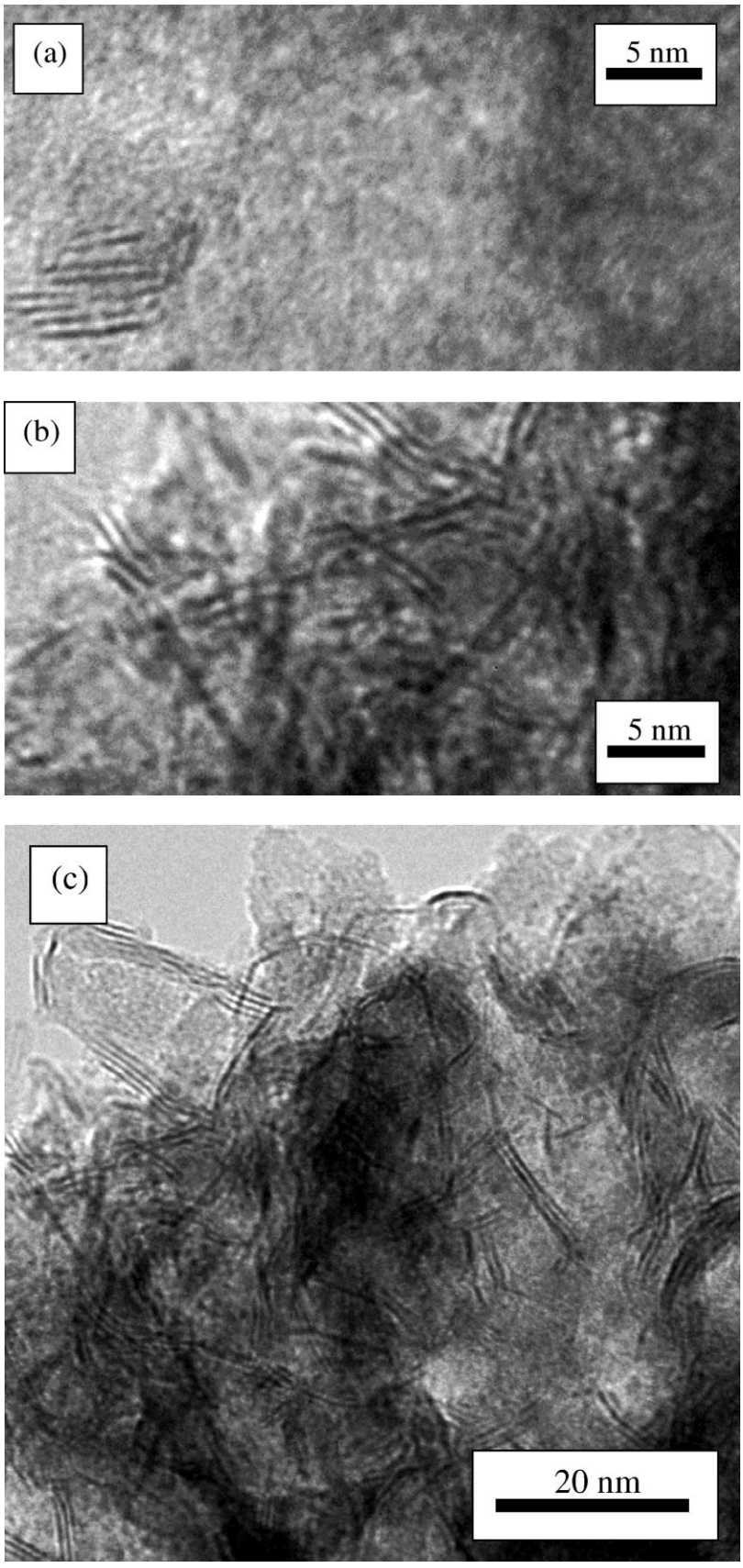

Figure 2. HR-TEM micrographs of Ni–W/SiO_2 (a) and Ni–W/Al_2O_3 ((b) and (c)) catalysts.

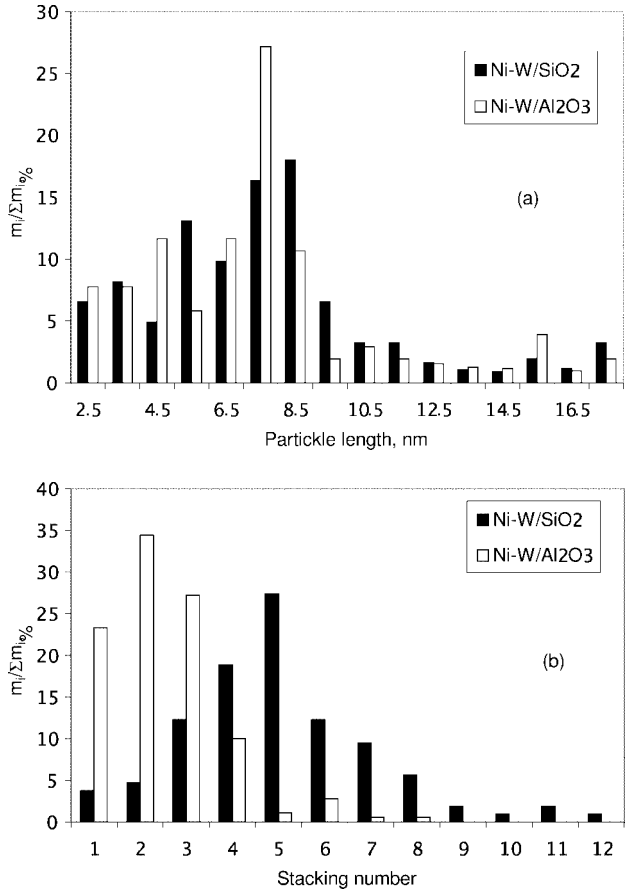

Figure 3. Comparison between the HR-TEM particle length (a) and stacking number (b) distribution of Ni–W/SiO_2 and Ni–W/Al_2O_3 catalysts.

reaction occurs mostly on the multilayered slabs. Similarly, Daage and Chianelli [4] concluded that the HDS reaction was catalyzed by both the rims and edges. However, opposite to our finding they concluded that HYD is catalyzed predominantly by rims. Daage and Chianelli [4] studied the performance of unsupported MoS_2 slabs. Recently, it was found that in supported MoS_2 systems the HYD rates increase with an increasing stacking degree [5], in agreement with our results.

Hensen *et al.* [5] found that a higher stacking degree improves also the intrinsic DBT HDS activity. We detected the same DBT HDS activity of both Ni–W/Al_2O_3 and Ni–W/SiO_2 catalysts (figure 1) that have different stacking number. This discrepancy is obviously a result of the fact that Hensen *et al.* [5] studied unpromoted MoS_2, while we studied the Ni-promoted WS_2 system. Indeed, it was found that the influence of Co and Ni promoters on alumina-supported MoS_2 is very different for the direct HDS and HYD reaction pathways of the DBT molecule [31,32]. The promoter causes a tremendous enhancement of the direct HDS pathway (C–S bond scission), while it has little effect on the HYD pathway. In our case with the promoted Ni–W system, DBT HDS occurred mainly via the direct HDS pathway in agreement with previous studies [24,33]. Therefore, we measured the same DBT HDS activity with Ni–W/SiO_2 and Ni–W/Al_2O_3.

In order to clarify the role of the stacking degree of the WS_2 slabs we estimated the chemisorption ability of Ni–W/SiO_2 and Ni–W/Al_2O_3 catalysts relative to toluene. Based on the integral intensity of the TCD signal, the amount of the substance desorbed at 400 °C is 1.8 times higher in case of Ni–W/SiO_2 compared with that for Ni–W/Al_2O_3. Assuming that such a stable molecule as toluene should not undergo any transformations at 400 °C in absence of hydrogen, it may be concluded that desorption of toluene is retarded on the Ni–W/SiO_2 catalyst compared with Ni–W/Al_2O_3. This could be considered as evidence of higher toluene adsorption strength on the Ni–W/SiO_2 catalyst compared with Ni–W/Al_2O_3 in agreement with the higher toluene HYD activity of the Ni–W/SiO_2 catalyst.

The results of the present study in line with previous studies [4,5] show the anisotropy of the W(Mo)S_2 slab layers. The HYD/HDS reactivity of the catalyst is controlled by the morphology of the W(Mo)S_2 phase. Furthermore, in case of the supported system the different morphologies are a consequence of the type of support and extent of metal–support interaction. It seems unlikely that W(Mo)S_2 multilayered slab contain other types of active sites than a single layer or thin slab, since the layers are not chemically bonded, but held together by van der Waals interactions. Therefore, the different performance of thin and thick W(Mo)S_2 slabs should be attributed to geometric considerations. Hensen *et al.* [5] attributed the increase of the HYD rate with increasing stacking degree of supported MoS_2 to less hampered planar adsorption geometry of reactants on multilayered MoS_2. Indeed, the necessary step of the direct HDS reaction is the adsorption of the thiophenic molecule (σ-bonding) in a predominantly perpendicular configuration on the single vacant site (coordinative unsaturated W(Mo) atom) [1]. Opposite to that, the aromatic molecule is adsorbed flat at anionic vacancies involving π-electrons of the aromatic ring. Considering the size of an aromatic ring, the π-complexation requires a higher adsorption area and involves multi vacancies on the catalyst surface [1]. The width of an aromatic ring (0.66 nm for benzene [34]) is enough to interact with at least two layers of W(Mo)S_2 slabs, since the Mo–Mo and W–W distances in the *c*-direction in the multilayered slab are both in the range of 0.61–0.62 nm [19]. The Mo–Mo distance within one layer of MoS_2 was estimated to be 0.32 nm [35] and the W–W distance is not much different from this value [36]. Each W(Mo) atom on the edges of the slab can potentially form an anionic vacancy when its sulfur atom leaves as hydrogen sulfide [1]. The actual amount of the vacancies depends on the process conditions (temperature, hydrogen sulfide partial pressure and so on). Therefore, aromatic ring multivacancy adsorption on the multilayered W(Mo)S_2 slab could occur potentially involving six vacancies in agreement with a consideration made by Topsøe *et al.* [1]. Opposite to that, on the single layer slab, only three vacancies could be potentially involved in the adsorption of the aromatic ring. Multilayered W(Mo)S_2 slabs provide a higher density of the multi vacancies compared with single-layered or thin slabs. This could facilitate π-complexation of the aromatic ring

on multilayered WS_2 slabs relative to single-layered or thin slabs in agreement with the TPD results. It enhances HYD activity of multilayered WS_2 slabs and, as a result, the silica-supported Ni–W catalyst having a higher stacking number displays a higher HYD activity than the Ni–W/Al_2O_3 catalyst.

4. Conclusions

The conditions which yield an optimized bulk Ni–W–S catalyst for aromatics hydrogenation, were employed for the first time for the preparation of supported Ni–W catalysts. They were prepared by impregnation of commercial γ-alumina and silica supports. The sulfidation, performed directly after drying at 100 °C, yielded fully sulfided Ni–W species on both supports (SEM-EDAX, XPS, XRD). At optimal metals loading ($\sim$50 wt% NiO + WO_3, Ni/W = 2), the sulfided catalysts had similar texture (N_2 adsorption) and displayed similar activity in dibenzothiophene hydrodesulfurization, while the activity of the Ni–W/SiO_2 catalyst in toluene hydrogenation was six times higher than that of Ni–W/Al_2O_3. The dispersion of Ni–W–S species is much higher on γ-alumina than on silica (XPS, XRD, TEM). This dispersion difference is a consequence of the more than two times thicker WS_2 slabs on the silica surface than that on γ-alumina with the same average slab length for both supports. The different WS_2 slab thickness goes band in band with a different number of layers (stacking number): more than two times higher on the silica surface than on γ-alumina. The desorption of toluene is retarded on the Ni–W/SiO_2 catalyst compared with Ni–W/Al_2O_3 (TPD). Multilayered WS_2 slabs provide a higher density of multi vacancies compared with single-layered or thin slabs facilitating the π-complexation of the aromatic ring. This enhances the hydrogenation activity of multilayered WS_2 slabs. The morphology of the Ni–W–S phase depends on the type of support and controls its activity in the hydrogenation of aromatic molecules.

References

[1] H. Topsøe, B.S. Clausen and F.E. Massoth, in: *Hydrotreating Catalysis*, eds. J.R. Anderson and M. Boudart (Springer, Berlin, 1996).

[2] D.D. Whitehurst, T. Isoda and I. Mochida, Adv. Catal. 42 (1998) 345.

[3] J.V. Lauritsen, S. Helveg, E. Laegsgaard, I. Stensgaard, B.S. Clausen, H. Topsøe and F. Besenbacher, J. Catal. 197 (2001) 1.

[4] M. Daage and R.R. Chianelli, J. Catal. 149 (1994) 414.

[5] E.J.M. Hensen, P.J. Kooyman, Y. van der Meer, A.M. van der Kraan, V.H.J. de Beer, J.A.R. van Veen and R.A. van Santen, J. Catal. 199 (2001) 224.

[6] O. Weisser and S. Landa, *Sulfide Catalysts, Their Properties and Applications* (Pergamon, London, 1973).

[7] L.N. Alexeenko, M.V. Landau, V. Ya. Kruglikov and B.K. Nefedov, Kinet. Katal. 25 (1984) 630.

[8] D.A. Agievskii, L.I. Pavlova, M.V. Landau, V.I. Kvashonkin and G.D. Chukin, Kinet. Katal. 26 (1986) 1042.

[9] M. Breysse, J. Bachelier, J.P. Bonnelle, M. Cattenot, D. Cornet, T. Decamp, J.C. Duchet, R. Durand, P. Engelhard, R. Frety, C. Gachet, P. Geneste, J. Grimblot, C. Gueguen, S. Kasztelan, M. Lacroix, J.C. Lavalley, C. Leclercq, C. Moreau, L. de Mourgues, J.L. Olivé, E. Payen, J.L. Portefaix, H. Toulhoat and M. Vrinat, Bull. Soc. Chim. Belg. 96 (1987) 829.

[10] H.R. Reinhoudt, A.D. van Langeveld, P.J. Kooyman, M. Stockmann, R. Prins, H.W. Zandbergen and J.A. Moulijn, J. Catal. 179 (1998) 443.

[11] H.R. Reinhoudt, E. Crezee, A.D. van Langeveld, P.J. Kooyman, J.A.R. van Veen and J.A. Moulijn, J. Catal. 196 (2000) 315.

[12] M.J. Vissenberg, Y. van der Meer, E.J.M. Hensen, V.H.J. de Beer, A.M. van der Kraan, R.A. van Santen and J.A.R. van Veen, J. Catal. 198 (2001) 151.

[13] C.H. Kim, W.L. Yoon, I.C. Lee and S.I. Woo, Appl. Catal. 144 (1996) 159.

[14] T. Kabe, W. Qian, A. Funato, Y. Okoshi and A. Ishihara, Phys. Chem. Chem. Phys. 1 (1999) 921.

[15] R.E. Tischer, N.K. Narain, G.J. Stiegel and D.L. Cillo, Prepr. Am. Chem. Soc. Div. Pet. Chem. 30 (1985) 459.

[16] Y. Yoshimura, T. Sato, H. Shimada, N. Matsubayashi, M. Imamura, A. Nishijima, M. Higo and S. Yoshitomi, Catal. Today 29 (1996) 221.

[17] C.D. Wagner, L.E. Davis, M.V. Zeller, J.A. Taylor, R.H. Raymond and L.H. Gale, Surf. Interface Anal. 3 (1981) 211.

[18] Powder Diffraction Files, JCPDS (International Center for Diffraction Data, 1984).

[19] E. Payen, R. Hubaut, S. Kasztelan, O. Poulet and J. Grimblot, J. Catal. 147 (1994) 123.

[20] G. Berhault, A. Mehta, A.C. Pavel, J. Yang, L. Rendon, M.J. Yacaman, L.C. Arazia, A.D. Moller and R.R. Chianelli, J. Catal. 198 (2001) 9.

[21] R. Burch and A. Collins, Appl. Catal. 18 (1985) 373.

[22] M.V. Landau, M. Herskowitz, D. Givoni, S. Laichter and D. Yitzhaki, Fuel 77 (1998) 3.

[23] M.V. Landau, L. Vradman, M. Herskowitz, Y. Koltypin and A. Gedanken, J. Catal. 201 (2001) 22.

[24] L. Vradman, M.V. Landau and M. Herskowitz, Catal. Today 48 (1999) 41.

[25] D. Briggs and M.P. Sean, *Practical Surface Analysis*, 2nd Ed., Vol. 1 (Wiley, New York, 1990).

[26] G. Kishan, L. Coulier, V.H.J. de Beer, J.A.R. van Veen and J.W. Niemantsverdriet, J. Catal. 196 (2000) 180.

[27] F.P.J.M. Kerkhof and J.A. Moulijn, J. Phys. Chem. 83 (1979) 1612.

[28] F.P.J.M. Kerkhof, J.A. Moulijn, R. Thomas and J.C. Oudejans, Stud. Surf. Sci. Catal. 3 (1979) 77.

[29] H. Hu, I.E. Wachs and S.R. Bare, J. Phys. Chem. 99 (1995) 10897.

[30] S.M.A.M. Bouwens, F.B.M. van Zon, M.P. van Dijk, A.M. van der Kraan, V.H.J. de Beer, J.A.R. van Veen and D.C. Koningsberger, J. Catal. 146 (1994) 375.

[31] F. Bataille, J.L. Lemberton, P. Michaud, G. Perot, M. Vrinat, M. Lemaire, E. Schulz, M. Breysse and S. Kasztelan, J. Catal. 191 (2000) 409.

[32] M. Breysse, G. Berhault, S. Kasztelan, M. Lacroix, F. Maugé and G. Perot, Catal. Today 66 (2001) 15.

[33] M.V. Landau, Catal. Today 36 (1997) 393.

[34] D.W. Breck, *Zeolite Molecular Sieves* (Wiley, New York, 1974).

[35] G. Plazenet, S. Cristol, J.F. Paul, E. Payen and J. Lynch, Phys. Chem. Chem. Phys. 3 (2001) 246.

[36] A.N. Startsev, Catal. Rev. Sci. Eng. 37 (1995) 353.